Absolute flow velocity components in laser Doppler flowmetry

Ingemar Fredriksson, Marcus Larsson and Tomas Strömberg

Ingemar Fredriksson, Marcus Larsson and Tomas Strömberg, Absolute flow velocity components in laser Doppler flowmetry, 2006, Proceedings of SPIE -- Volume 6094 Optical Diagnostics and Sensing VI.
http://dx.doi.org/10.1117/12.659206.

Absolute flow velocity components in laser Doppler flowmetry

Ingemar Fredriksson*, Marcus Larsson and Tomas Strömberg
Department of Biomedical Engineering, Linköping University, 581 83 Linköping, Sweden

ABSTRACT

A method to separate a Doppler power spectrum into a number of flow velocity components, measured in absolute units (mm/s), is presented. A Monte Carlo software was developed to track each individual Doppler shift, to determine the probability, $p(n)$, for a photon to undergo n Doppler shifts. Given this shift distribution, a mathematical relationship was developed and used to calculate a Doppler power spectrum originating from a certain combination of velocity components. The non linear Levenberg-Marquardt optimization method could thus be used to fit the calculated and measured Doppler power spectra, giving the true set of velocity components in the measured sample. The method was evaluated using a multi tube flow phantom perfused with either polystyrene microspheres or undiluted/diluted human blood ($hct = 0.45$). It estimated the velocity components in the flow phantom well, during both low and high concentrations of moving scatterers (microspheres or blood). Thus, further development of the method could prove to be a valuable clinical tool to differentiate capillary blood flow.

Keywords: Laser Doppler flowmetry, LDF, Monte Carlo simulations, flow phantom, blood perfusion, scattering phase function, red blood cell

1. INTRODUCTION

Laser Doppler flowmetry (LDF) is a technique to measure the blood perfusion in the microcirculation, i.e. the capillaries, venules and arterioles.[1] A drawback with LDF is that it has not been possible to measure the perfusion in absolute units, nor has it been possible to differentiate between the principal types of blood flow; arteriolar, venular and capillary flow.[1,2] Most often, from a physiological point of view, the nutritive capillary blood flow is of greatest interest. However, since the velocity of the deeper and larger vessels is much higher, the perfusion signal contribution from these vessels dominates over the contribution from the capillaries. Consequently, the LDF measurements often contain little information about the physiologically interesting capillary blood flow.

A previous study has shown that the LDF signal can be separated into at least three different velocity regions by decomposing the Doppler power spectrum.[3] That approach, however, did not include multiple Doppler shifts, which is likely to be found in most tissues. Another approach to differentiate blood flow of different velocities and types has been presented by Dörschel and Müller[4], who developed a method to correct the Doppler power spectrum to obtain a relationship between certain frequency regions and corresponding velocities. They assumed an isotropic angle distribution between the scattering vector and the red blood cell (RBC) velocity, and a constant scattering angle. However, the assumption of a constant scattering angle is too rough and the method does not consider multiple Doppler shifts. Koelink *et. al.*[5] used two different wavelengths and two different source-detector separations to distinguish the microcirculation from the deeper situated blood vessels, but the method was only able to roughly separate the two types of flow. Various methods[6-8] have been presented that estimate the average RBC velocity by comparing measured and simulated spectra. The source-detector distance was however large in these methods (> 15 mm) and they could only estimate the average velocity, not separate different velocity regions.

The method presented here aims to differentiate various blood flow velocity components found in the LDF signal. The principle is to decompose the LDF spectrum, assumed to originate from photons that are multiple Doppler shifted to some degree, into several velocity regions. This is done by fitting a combination of reference spectra, each based on one of those velocity regions, to the measured spectrum. Monte Carlo simulations are employed to estimate the degree of multiple shifted photons. Potentially, this method could be used *in vivo* to isolate the low velocity capillary blood flow.

* Email: ingfr@imt.liu.se; Phone: +46-13-222483; Fax: +46-13-101902

2. MATERIAL AND METHODS

2.1. LDF spectrum

When a photon is scattered by a moving particle, a small frequency shift, or Doppler shift, will occur. A single Doppler scattering event is shown in figure 1, where $\mathbf{k_i}$ is the vector of the incident photon, $\mathbf{k_s}$ is the vector of the scattered photon, θ is the scattering angle and ϕ is the angle between the scattering vector $\mathbf{q}$ and the velocity vector $\mathbf{v}$ of the particle. The resulting Doppler shift (β_d) is defined by[1]

$$\beta_d = \mathbf{q} \cdot \mathbf{v} = \frac{4\pi}{\lambda_t} \cdot \sin(\theta/2) \cdot v \cdot \cos\phi\,, \tag{1}$$

where λ_t is the wavelength in the medium. In most situations θ, ϕ and $\mathbf{v}$ are described by distributions, and therefore, the detected photons will have been shifted with a variety of frequencies, resulting in an optical Doppler spectrum ($I(\beta)$) as shown in figure 2. For a 786 nm Laser source with a center frequency, β_c, of 390 THz, a maximum shift, $\Delta\beta$, of approximately 5 kHz (i.e. a relative shift of $1.3 \cdot 10^{-11}$) can be expected in ordinary tissue ($v \in [0\ 5]$ mm/s).

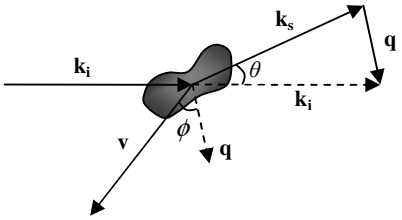

Figure 1: Doppler scattering event

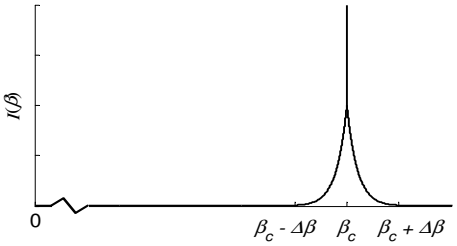

Figure 2: Optical Doppler spectrum

Back scattered photons that have been partly Doppler shifted form a fluctuating speckle pattern on the detector. The frequency content of the resulting detector current is linked to the frequency shifts of the detected photons, i.e. the optical Doppler spectrum $I(\beta)$, as[9,10]

$$P(\omega) = q_{ac} I(\beta) \star I(\beta), \quad \omega \leftarrow \left|\beta - \beta_c\right|, \tag{2}$$

where q_{ac} is an instrumental constant and $\star$ denotes the cross correlation. From now on, $P(\omega)$ is referred to as the *Doppler power spectrum*, in contrast to the *optical Doppler spectrum* $I(\beta)$.

Since each Doppler shift is proportional to the velocity of the scattering particle, the width of the Doppler power spectrum is directly proportional to the velocity content of the sample. An increased velocity of the flow could thus be seen as a broadening of the spectrum. When the concentration increases, two effects take place. Foremost, the fraction of detected photons that have been Doppler shifted increases, which increases the total power of the spectrum (outside the zero frequency). When the concentration increases even more, a relatively large fraction of the detected photons will be Doppler shifted more than once. This will also result in a broadening of the optical Doppler spectrum and hence, it can be difficult to distinguish a high velocity from a high concentration of moving scatterers.

2.2. Mathematical derivation of multiple Doppler shifted spectrum

To discriminate various velocity regions using Doppler power spectra that originate from multiple Doppler shifted photons, a mathematical connection between such spectra and single shifted optical Doppler spectra from specific velocity regions is needed. A multiple shifted Doppler power spectrum with i velocity regions, or velocity components, can be expressed with equations 3 to 6. The optical Doppler spectra presented below are centered around zero, i.e. $\beta \leftarrow \beta - \beta_c$ where β_c is the center frequency. The first equation expresses the single shifted optical Doppler spectrum

$$I_1(\beta) = \sum_{v_i} c_{v_i} I_{v_i}(\beta)\,, \tag{3}$$

where c_{v_i} is the velocity components and $I_{v_i}(\beta)$ is the optical Doppler spectrum for velocity region v_i. The optical spectrum of photons shifted n times can be calculated by successive cross correlations

$$I_n(\beta) = I_1(\beta) \star I_{n-1}(\beta) . \tag{4}$$

To calculate the combined multiple shifted optical spectrum, the probability distribution of the number of times a photon is scattered by a moving particle, $p(n)$, must be known. Serov with colleagues suggest that under the assumption that the media examined is homogenous with evenly distributed moving scatterers, this distribution can be well approximated by a Poisson distribution.[11] For the general case though, this can not be assumed and the distribution is therefore found empirically via Monte Carlo simulations. For a known distribution, the multiple shifted optical spectrum is expressed by

$$I_{ms}(\beta) = \sum_n p(n) I_n(\beta) . \tag{5}$$

The calculated Doppler power spectrum ($P_{calc}(\omega)$) is the auto correlation of this multiple shifted optical spectrum, according to equation 2,

$$P_{calc}(\omega) = I_{ms}(\beta) \star I_{ms}(\beta), \quad \omega \leftarrow |\beta| . \tag{6}$$

Due to the successive cross correlation in equation 4, the computation is time consuming. In order to increase the computation speed, the calculations can be performed in the Fourier domain. Let $Y_1(x)$ be the Fourier transform of $I_1(\beta)$,

$$Y_1(x) = \mathcal{F}\{I_1(\beta)\} . \tag{7}$$

The cross correlation can be written as a convolution since the optical Doppler spectra are centered and assumed symmetric around zero. Furthermore, the convolution is analogue to a multiplication in the Fourier domain, and equation 4 is therefore rewritten as

$$Y_n(x) = Y_1(x) \cdot Y_{n-1}(x) = Y_1^n(x) . \tag{8}$$

The Fourier transform is linear and the Fourier domain analogue to equation 5 can therefore be written as

$$Y_{ms}(x) = \sum_n p(n) Y_n(x) = \sum_n p(n) Y_1^n(x) . \tag{9}$$

Finally, equation 6 is rewritten as

$$P_{calc}(\omega) = I_{ms}(\beta) \star I_{ms}(\beta) = \mathcal{F}^{-1}\{(Y_{ms}(x))^2\}, \quad \omega \leftarrow |\beta| . \tag{10}$$

2.3. Scattering phase function

As seen in equation 1, the scattering angle θ greatly affects the size of the Doppler shifts. Accordingly, strongly forward scattering particles result in small Doppler shifts and narrow spectra, whereas more isotropic scattering particles result in larger Doppler shifts and wider spectra. The scattering angle of a particle is determined by its phase function, which in turn is affected by the size and shape of the particle and the difference in refractive index between the particle and the surrounding medium. For microspheres, Mie theory can be used to predict the phase function given those parameters.[12]

Polystyrene microspheres (motility standard PF 1001, Perimed AB, Järfälla, Sweden), with a radius of 0.155 µm and a refractive index of 1.58 at 786 nm, were used as scatterers in the first part of this study. The microspheres were suspended in various concentrations in deionized water with a refractive index of 1.33 at 786 nm. The phase function of the polystyrene spheres was calculated using Mie theory, yielding an anisotropy factor ($g = < \cos \theta >$) of 0.494.

In the second part of the study, RBC:s were used as scatterers. RBC:s are complex in shape and therefore the use of Mie theory may not be applicable[13]. Thus, we used the empirical two parametric Gegenbauer kernel phase function[14]

(equation 11) for the RBC:s which according to Hammer *et. al.*[15] and Roggan *et. al.*[16] can be applied to approximate the phase function of RBC:s, at least at low concentrations.

$$p_{Gk}(\theta) = \frac{\alpha_{Gk} g_{Gk} (1 - g_{Gk}^2)^{2\alpha_{Gk}}}{\pi((1 + g_{Gk})^{2\alpha_{Gk}} - (1 - g_{Gk})^{2\alpha_{Gk}})(1 + g_{Gk}^2 - 2g_{Gk}\cos(\theta))^{\alpha_{Gk}+1}} \tag{11}$$

We used a method, similar to that described by Kienle *et. al.*[17], to determine the parameters of the Gegenbauer kernel phase function of an RBC. Measured blood Doppler power spectra were fitted to spectra calculated via equations 3, 7-10, where the shift distribution $p(n)$ in equation 9 were given by a Monte Carlo simulation using a phase function close to the finally estimated. The use of this approximate phase function to determine $p(n)$ is possible since a small change of the phase function has a minimal impact on the shift distribution.[17] The optical Doppler spectrum $I_{v_i}(\beta)$ in equation 3 were calculated for each set of g_{Gk} and α_{Gk}, and the χ^2 error

$$\chi^2 = \sum \left(1 - \frac{P_{calc}}{P_{meas}} \right)^2 \tag{12}$$

were minimized to reach the phase function that resulted in a least square fit.

2.4. Velocity decomposition

A velocity region should be defined to roughly reflect the velocity distribution of a typical type of flow. For the two measurement series in this study, the velocity regions were chosen to reflect a flow of evenly distributed particles of a parabolic flow profile. As a consequence, the velocity of the moving scatterers was evenly distributed between zero and twice the mean velocity. For the measurements with polystyrene spheres, the mean velocities were chosen to be 0.5, 2.0 and 8.0 mm/s respectively, and for the blood measurements 1.0, 5.0 and 15.0 mm/s.

For a given velocity component, a single shifted optical Doppler spectrum was calculated using a fast and simple Monte Carlo[18] algorithm. In the algorithm, each photon was Doppler shifted once, and it was assumed that the angle between the incident photon and the scattering particle was isotropic. Furthermore, the velocity of each particle was randomly chosen between zero and twice the mean velocity of the particles, mimicking a parabolic flow profile.

In order to fit the velocity components c_{v_i} to the measured spectrum P_{meas}, the non-linear Levenberg-Marquardt method[19] was employed. The χ^2 merit function was

$$\chi^2 = \sum \left(1 - \frac{P_{calc}}{P_{meas}} \right)^2 \tag{13}$$

where P_{calc} is the calculated multiple shifted Doppler spectrum for the components c_{v_i} in each iteration. Any component that received a value below zero was set to zero and a new fit were performed with the other components. This was repeated until all components were zero or positive. Ideally, the sum of all velocity components should be 1.0 (note that the shift distribution $p(n)$ in equation 9 can contain a large part of zero shifts). Therefore, the velocity components are finally multiplied with the fraction of shifted photons and the result can be interpreted as *the relative concentration of scatterers in the sample flowing with a velocity specified by velocity region i.*

2.5. Measurement system

The measurements were performed with a Periflux 5000 system (Perimed AB, Järfälla, Sweden). The laser source in the system was a diode laser at 786 nm, coupled to a standard optic probe (Probe 408, Perimed AB, Järfälla, Sweden). The probe (figure 3) consisted of one emitting and one receiving step-index fiber, both having a core diameter of 125 µm and a numerical aperture of 0.37. They were separated 230 µm apart (centre to centre distance) at the probe tip. The system was modified by Perimed AB to give the two output signals ac_m (time varying signal) and dc_m (total light intensity), where the ac_m signal was amplified and band-pass filtered between 8 Hz and 20 kHz, and the dc_m signal was amplified and low-pass filtered using a cut-off frequency of 32 Hz. Both signals were sampled at 50 kHz using a 12-bit AD-card (DAQpad-6070E, National Instruments Inc.).

Matlab 7.0 (MathWorks Inc.) was used for the digital data processing and the inbuilt method to estimate the power spectral density were used to get the Doppler power spectrum from the measurement. A more detailed description of the data processing have been presented by Larsson and Strömberg.[3]

2.6. Flow phantom

A flow phantom, shown in figure 4, was built to evaluate the method. It consisted of a polythene micro-tube wrapped around a piece of delrin. The micro-tube had an outer radius of 0.50 mm and an inner radius of 0.25 mm. The gaps between the tube wrappings were filled with transparent silicone. Another piece of delrin was placed on top of the tubes in order to make the light more isotropic before the interaction with the flow.

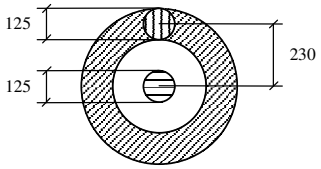

Figure 3: Source-detector geometry. Horizontal lines: source. Vertical lines: measurement detector. Diagonal lines: MC detector. Measures in µm.

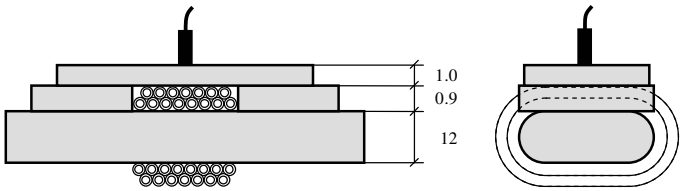

Figure 4: Schematic view of the flow model. The gray areas were made of delrin and the gaps between the tube wrappings were filled with transparent silicone. The probe is shown at the top. Measures in mm.

The scattering coefficients of delrin, tube wall and silicone were approximated to 24, 1.0 and 2.0 mm^{-1}, respectively, and an absorption coefficient of 0.02 mm^{-1}, a refractive index of 1.47 and an anisotropy factor of 0.9 were approximated for all materials. Furthermore, the Henyey-Greenstein phase function[20] was assumed for all materials.

The motility standard was assumed non-absorbing at 786 nm while the scattering coefficient was measured using a collimated transmission setup, yielding scattering coefficients between 0.12 and 1.92 mm^{-1} for the dilutions used in the measurements.

For blood, the absorption coefficient was calculated by

$$\mu_a = C \cdot hct \cdot \rho / m \cdot (S\mu_a^{HbO_2} + (1-S)\mu_a^{Hb}). \quad (14)$$

Here, *hct* is the hematokrit (volume fraction of RBC:s), S is the oxygen saturation (approximated to 0.8), $\mu_a^{HbO_2}$ and μ_a^{Hb} are the absorption coefficients of oxygenated and deoxygenated hemoglobin, respectively, tabulated by Prahl[21] (74 and 96 mm^{-1}/(mol/l) at 786 nm). Furthermore, ρ is the density of hemoglobin in RBC:s (343 g/l)[22], m is the molecule mass of hemoglobin (64500 g/mol)[21] and C is a constant added to compensate the increased pathlength of the light in the RBC:s (2 [dimensionless])[16,21]. For a normal hematokrit of 0.45, μ_a equals 0.38 mm^{-1} at 786 nm.

Determining the scattering coefficient of blood is difficult due to aggregation effects of blood of physiological hematokrit.[13,16] However, the approximation

$$\mu_s = \frac{hct(1-hct)}{V}\sigma_s \quad (15)$$

was derived by Twersky[23] for densely packed scatterers, where V is the volume of a single scatterer and σ_s is the scattering cross section. For blood, V is ~90 μm^3 and σ_s is approximated to 57.5 μm^2 at 786 nm, yielding a scattering coefficient of 158 mm^{-1}.[15,16] In the measurements, blood of a hematokrit of about 0.45 was used. The blood was heparinized to minimize the risk of coagulation and diluted in physiological saline (0.9 % NaCl).

A syringe pump (Orion Sage pump M362, Thermo Electron Corporation) was used to achieve well-controlled flow in the micro tube.

2.7. Monte Carlo simulations

A Monte Carlo (MC) software based on Prahl *et. al.*[18] and Wang *et. al.*[24], with the possibility to simulate Doppler shifts[25,26], was developed. The software supported multiple layers, various geometrical objects (such as cylinders and tubes), various phase functions (Henyey-Greenstein, Gegenbauer kernel and Mie) and flows with various flow profiles.

The phantom geometry presented in the previous section was set up in the Monte Carlo software. The source and the detector followed the probe geometry used in the measurements, with two exceptions, both leading to more detected photons in the simulations; 1) the detector was configured as a ring with an inner radius of 0.1675 mm and an outer radius of 0.2925 mm with its center in the center of the emitter, see figure 3; 2) the numerical aperture of the detector was increased to 1.0. Simulations showed that the shape of the Doppler power spectrum did not change with these two exceptions.

For each simulation, 25-250 million photons were emitted and about 1 to 5 percent of these were detected. For each detected photon, the number of Doppler shifts and the total Doppler shift were recorded, and for each Doppler shift of a detected photon, the shift number and the shift frequency (β_d) were recorded. This resulted in a simulated optical Doppler spectrum which were calculated to a Doppler power spectrum according to equation 6. The purpose of the simulations was to reveal the shift distribution, $p(n)$, used in the calculations in section 2.2, and to be used as a comparison to the measured and calculated spectra, respectively. The simulated spectra should thus not be confused with the calculated spectra (P_{calc}).

3. RESULTS

3.1. Polystyrene spheres

Measured laser Doppler spectra and shift distributions from simulations of four different concentrations of polystyrene spheres are shown in figures 5 and 6. As predicted in section 2.1, the total energy increases for higher concentrations and the spectra also broadens slightly for higher concentrations. As expected, the fraction of shifted photons and the number of multiple shifts increase with concentration.

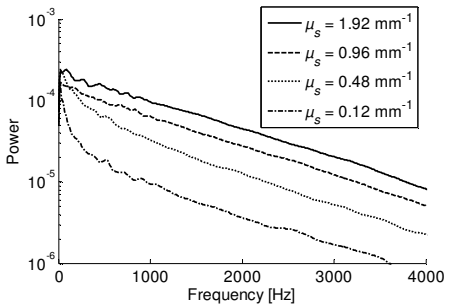

Figure 5: Measured Doppler power spectra for various concentrations of polystyrene spheres, v = 1.0 mm/s.

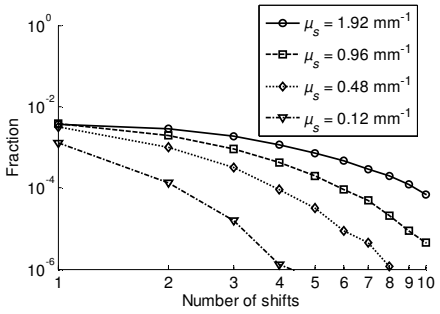

Figure 6: Shift distributions for various concentrations of polystyrene spheres. The fraction of unshifted photons were 0.9986, 0.9953, 0.9925 and 0.9886, respectively.

According to equation 1, the Doppler shifts are linearly proportional to the velocity. Thus, re-scaling the frequency with the velocity should lead to nearly identical spectra for all velocities of the same concentration. Such frequency re-scaling has been performed in figure 7. The figures show that the re-scaled spectra are not identical; spectra that originate from high velocities appear as if they were generated by a slightly lower velocity, and there is also a tendency that the total energy decreases with the velocity. The figure also contains Monte Carlo simulations of the same concentrations, which are in good agreement with the low velocity spectra. The same phenomena can be observed for all concentrations.

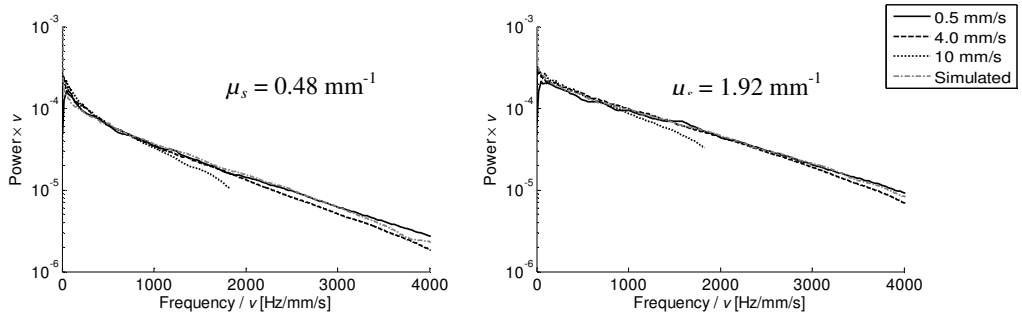

Figure 7: Laser Doppler spectra for various velocities with polystyrene spheres, where the frequency is re-scaled with the velocity.

Measured, simulated and calculated spectra for the polystyrene spheres with μ_s = 0.48 and 1.92 mm^{-1}, v = 1.0 mm/s, are shown in figure 8. The measured and simulated spectra coincide well, whereas the calculated spectrum is slightly wider than the other two for the higher concentration.

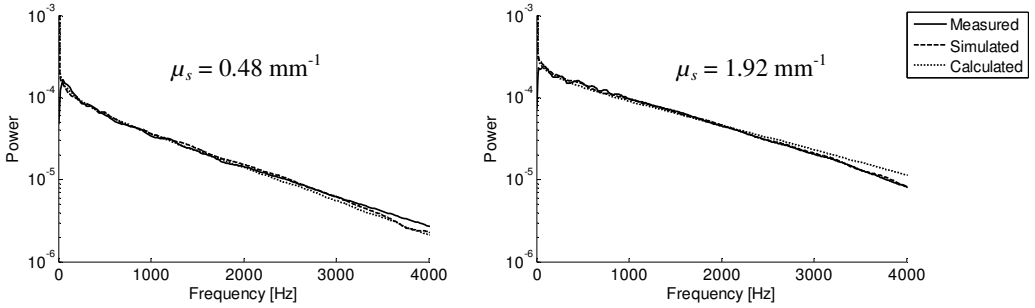

Figure 8: Measured, simulated and calculated spectra for polystyrene spheres, v = 1.0 mm/s.

For the measurements of the polystyrene sphere suspensions with μ_s = 0.48 and 1.92 mm^{-1}, a fraction of 0.0047 and 0.0114 of the detected photons had been Doppler shifted, respectively. Decompositions of these measurements, using the flow regions 0.5, 2.0 and 8.0 mm/s (mean velocity), are presented in figure 9. The expected result was that the measurements at 0.5, 2.0 and 8.0 mm/s should only consist of the respective flow component. However, due to measurement uncertainties and the discrepancies between the measured, simulated and calculated spectra presented above, the mean velocity is estimated to be lower than the actual mean velocities in the flow phantom. The underestimation also seems to be more legible for the higher concentration.

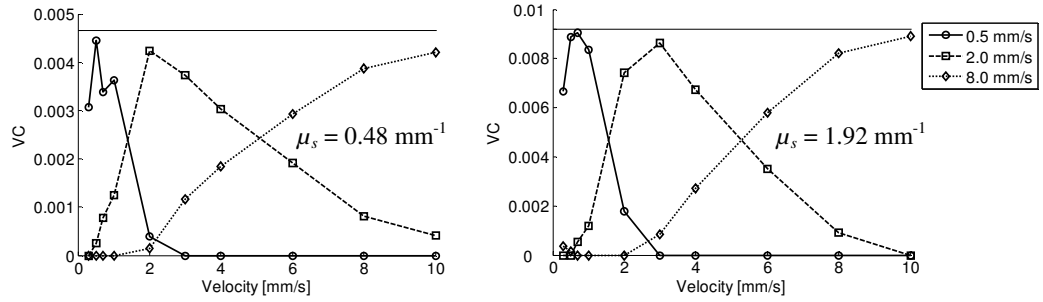

Figure 9: Fitted velocity components for polystyrene sphere measurements. The fraction of Doppler shifted photons is 0.0047 and 0.0114, respectively (the horizontal lines).

3.2. Blood

Measured laser Doppler spectra and the shift distributions from MC simulations for the four different blood concentrations are shown in figures 10 and 11. Here, the frequency broadening due to multiple shifts is legible, which follows naturally since most shifted photons have been shifted tens or hundreds of times for the high concentrations.

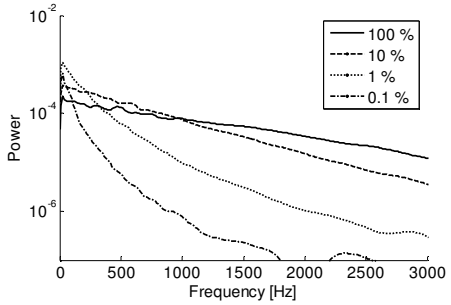

Figure 10: Measured Doppler power spectra for various concentrations of blood, v = 1.0 mm/s.

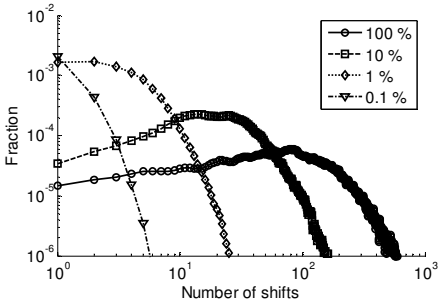

Figure 11: Shift distributions for various concentrations of blood. The fraction of unshifted photons were 0.9974, 0.9916, 0.9907 and 0.9890, respectively.

Figure 12 shows velocity re-scaled Doppler power spectra from the four different blood concentrations. Just as in the case of the polystyrene spheres, the spectra of high velocities are narrower than expected. That is most obvious in the case of 100 % blood, but the effect exists for all concentrations. For 0.1 % blood for example, the difference between the power at the re-scaled frequency of 100 and 500 Hz/mm/s is about 15 % larger for 15 mm/s than for 1.0 mm/s.

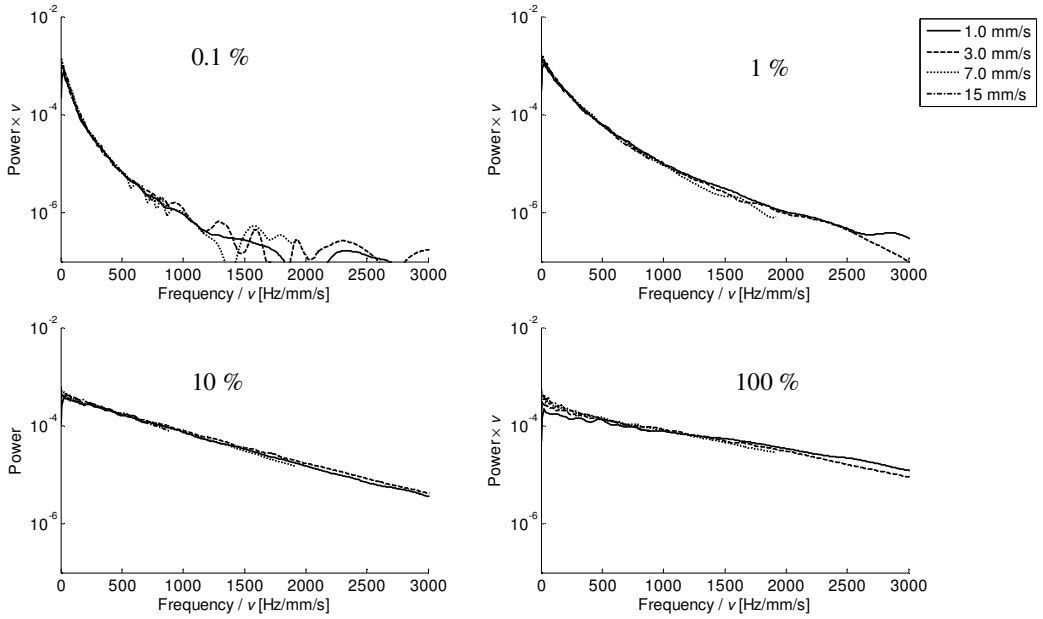

Figure 12: Velocity normalized LDF spectra of four different velocities and four different concentrations.

As seen in the case with polystyrene spheres, the simulations and measurements agree best for low velocities and low concentrations. Thus, the two parametric Gegenbauer kernel phase function was fitted to the measured spectra with low velocities (0.5-2.0 mm/s) and low concentrations (0.1 and 1.0 %). The fitted phase functions agreed well with each other, and the resulting parameters were determined to α_{Gk} = 1.00 and g_{Gk} = 0.937, giving an anisotropy factor $g = <\cos\theta>$ of 0.988, i.e. strongly forward scattering.

Using the fitted phase function, spectra were simulated and calculated for the various blood concentrations. The results, together with the measured spectra for v = 1.0 mm/s, are shown in figure 13. The measurements, simulations and calculations coincide well for this low velocity for the two lowest concentrations. In the case of 10 % blood, the measurement seems to originate from a slightly lower velocity compared to the simulation and calculation. For 100 %,

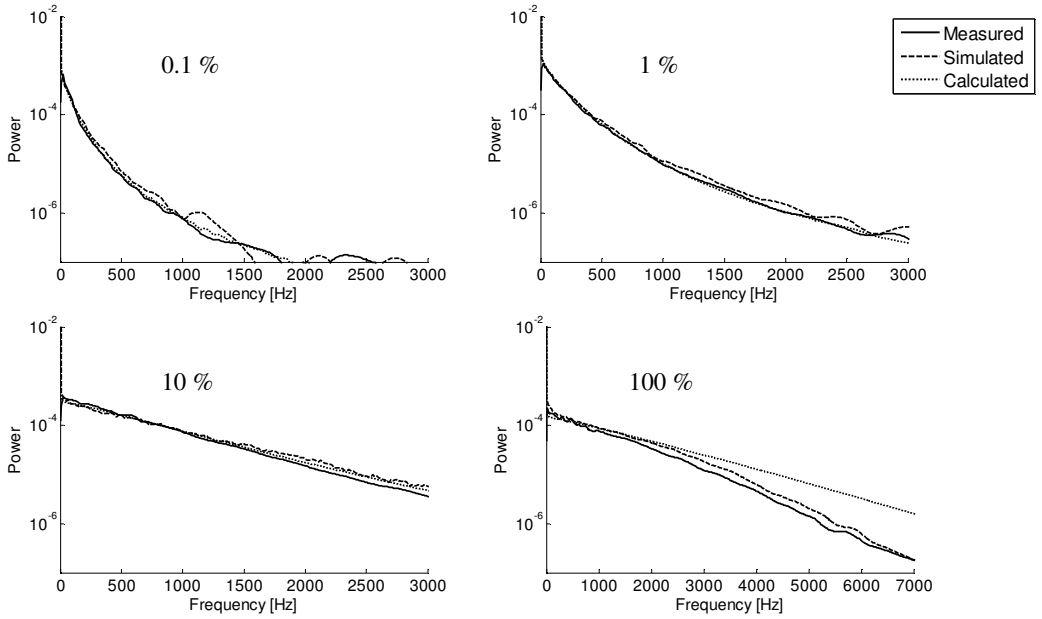

Figure 13: Measured, simulated and calculated spectra for blood, v = 1.0 mm/s.
Note the difference in the frequency scale for 100 %.

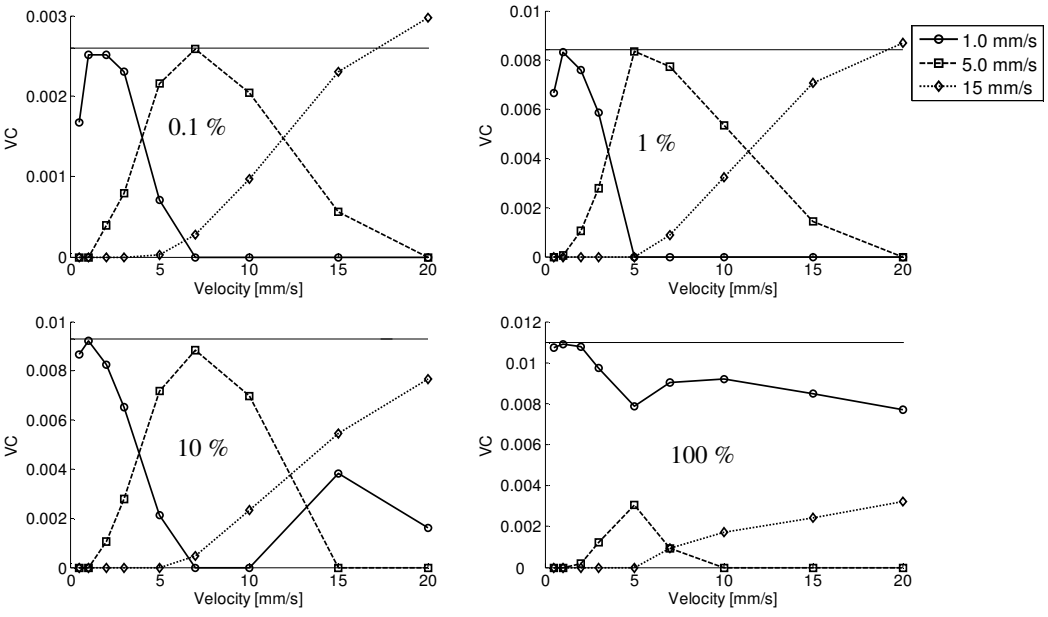

Figure 14: Velocity components versus mean flow velocity for four different blood concentrations.
The fractions of Doppler shifted photons (marked in the figures) were: 0.0026, 0.0084, 0.0093 and 0.0110, respectively.

the most obvious is that the calculation differs significantly from the simulation and measurement, it appears that the calculation originates from a significantly higher velocity.

The decomposed velocity components from the blood measurements are shown in figure 14. The fraction of Doppler shifted photons were 0.0026, 0.0084, 0.0093 and 0.0110, respectively. An underestimation of the velocities can be observed.

4. DISCUSSION

For both polystyrene spheres and blood, the measurements for the high velocities result in narrower spectra than expected, as seen in figures 7 and 12. The total energy in the spectra also seems to decrease with increased velocity. These two effects are the same as the effects of a lower scattering coefficient, as stated in section 2.1. Roggan *et. al.*[16] observed that the absorption coefficient as well as the scattering coefficient of blood seemed to decrease for increased shear rates. They also concluded that the effect was due to axial migration of the RBC:s, which is a well known behavior of many types of suspensions[27,28]. Furthermore, the geometry of the flow phantom used in the measurements introduces an uncertainty of both the particle distribution and the velocity profile due to the wrappings of the tube. Thus, we argue that the effect of narrower spectra for high velocities is due to an uneven cross-sectional distribution of particles in the tube and/or small changes of the velocity profile with changed mean velocity. Consequently, the shift distribution originating from the MC simulations will differ slightly from the true shift distribution which in turn leads to the underestimation of the velocity components observed in figures 9 and 14.

For high concentrations of both polystyrene spheres and blood, the underestimation of the velocity components is also caused by other effects. As seen in figures 8 and 13, the calculated spectra differ from the measured and simulated, for the highest concentrations. However, the reason of this differs. For the polystyrene spheres, a photon that is shifted multiple times within the same tube tends to change shift direction for each shift, and therefore the optical spectrum becomes narrower than if the shift direction was completely random. The reason they tend to change direction can be understood by studying the three scattering cases in figure 15. In the figure, the flow direction is from left to right. A photon with an incident angle marked by the solid arrow in the left figure can be scattered in any direction. If it is scattered within the dark gray circle sector, the resulting Doppler shift is positive, as in case a. The probability that the next shift is also positive then decreases, and the opposite is true for a negative shift, where the probability that the next shift is also negative decreases, as in case b. The same reasoning holds for all angles and in three dimensions. However, this is not taken into account in the calculations and therefore the calculated spectrum differs from the measured and simulated, which contributes to the underestimation of the velocity components.

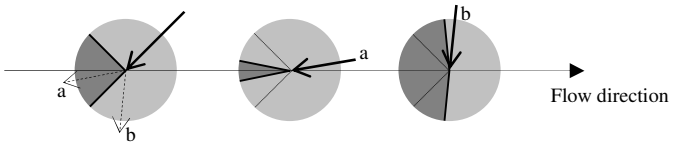

Figure 15: The reason two succeeding shifts tend to change direction. A scattering angle within the dark gray sectors results in a positive shift and within the light gray sectors results in a negative shift.

This effect is significant for rather isotropic scattering particles, such as the polystyrene spheres with an anisotropy factor of 0.494. However, for strongly forward scattering particles, such as blood with an anisotropy factor of 0.988, the probability of a shift in either direction is always close to 50 %. The reason that the calculations differ from the simulations and measurements in this case is that the Doppler shifts occur near the wall of the tube to a greater extent, caused by the high scattering coefficient of blood. Since the velocity is lower near the wall (parabolic flow profile) the spectra become narrower than if the shifts would have occurred uniformly over the whole area of the tube. This effect is interesting when inspecting the velocity components of whole blood in figure 14. The low velocity component is dominating for all flow velocities in that case which is correct since most Doppler shifts are caused by RBC:s with low velocity near the tube wall. For the same reason, the low velocity component is visible for the high velocities for the decompositions of 10 % blood.

These three effects all contribute to an underestimation of the velocity components, more legible for higher velocities and concentrations. Other sources of error which could affect the results are the uncertainties of the optical properties of the flow phantom, uncertainty of the probe placement (on top of one wrapping or in between two), perturbations in the static flow, sedimentation, and uncertainties of the exact optical properties of blood. However, the impact of these errors and uncertainties is probably less than the impact of the effects presented above.

The shift distribution of the detected photons is essential in the presented method. For the flow phantom used in this study, a proper shift distribution could be resolved by simulations. For *in vivo* measurements on the other hand, that can not be done since the structure and optical properties of tissue varies both between individuals and locally for the same individual. Serov *et. al.*[11] suggest that the shift distribution follows a Poisson distribution for a homogeneous medium, and the distribution could thus be calculated with knowledge of the fraction of Doppler shifted photons. However, they also suspect that the assumption of homogeneity is too rough for most tissues. To generalize the presented method to *in vivo* measurements, a method to estimate the shift distribution, based on empirical data, must therefore be developed. In regions with a high volume fraction of blood (i.e. high degree of multiple Doppler shifts), the accuracy of the derived velocity components will strongly depend on the accuracy of this estimation.

The geometry of tissue will however lead to a number of simplifications in comparison to the phantom as well. First, the homogeneity of tissue is much higher than in the case of the phantom, with respect to the whole sample volume. That leads to the possibility to approximate an accurate shift distribution, which would probably be impossible for the flow phantom without an exact knowledge about its structure. Secondly, the blood vessels comprising the microcirculation are much smaller than the tube used in the flow phantom. That will eliminate the problem that more Doppler shifts occur near the walls giving a misleading approximation of the flow. Finally, the blood flows in all possible directions in the microcirculation, justifying the isotropic assumption between the photons and the flow direction even without something that diffuses the light like the 1 mm piece of delrin used in the flow phantom.

5. CONCLUSIONS

We have shown that it is possible to accurately decompose a laser Doppler spectrum originating from multiple Doppler shifted photons into a number of predefined velocity regions for a well defined flow phantom. Many of the problems encountered during the work are bound to the special characteristics of the flow phantom and will thus not arise for *in vivo* skin measurements. Thus, the method could be valuable for *in vivo* measurements, which however still is to be evaluated.

6. ACKNOWLEDGEMENTS

The authors are grateful to Perimed AB for valuable co-operation and support. The project was supported by the Swedish Agency for Innovation Systems (VINNOVA) through the Swedish National Board of Excellence for Non-Invasive Medical Measurements (NIMED).

REFERENCES

1. G.E. Nilsson, E.G. Salerud, N.O.T. Strömberg, and K. Wårdell, "Laser Doppler Perfusion Monitoring and Imaging", *Biomedical photonics handbook*, T. Vo-Dinh, 15-1 - 15-24, CRC Press, Boca Raton, FL, 2003
2. M.J. Leahy, F.F. De Mul, G.E. Nilsson, and R. Maniewski, "Principles and practice of the laser-Doppler perfusion technique", Technology and Health Care, **7**(2-3), 143-62, 1999
3. M. Larsson and N.O.T. Strömberg, "Towards a velocity resolved microvascular blood flow measure by decomposition of the laser Doppler spectrum", Accepted for publication in Journal of Biomedical Optics, 2005
4. K. Dörschel and G. Müller, "Velocity resolved laser Doppler blood flow measurements in skin", Flow Measurement and Instrumentation, **7**(3-4), 257-264, 1996
5. M.H. Koelink, F.F.M. De Mul, *et al.*, "Laser-Doppler Blood Flowmetry Using two Wavelengths - Monte-Carlo Simulations and Measurements", Applied Optics, **33**(16), 3549-3558, 1994

6. R. Lohwasser and G. Soelkner, "Experimental and theoretical laser-Doppler frequency spectra of a tissuelike model of a human head with capillaries", Applied Optics, **38**(10), 2128-2137, 1999
7. A. Kienle, "Non-invasive determination of muscle blood flow in the extremities from laser Doppler spectra", Physics in Medicine and Biology, **46**(4), 1231-44, 2001
8. T. Binzoni, T.S. Leung, D. Boggett, and D. Delpy, "Non-invasive laser Doppler perfusion measurements of large tissue volumes and human skeletal muscle blood RMS velocity", Physics in Medicine and Biology, **48**(15), 2527-2549, 2003
9. A.T. Forrester, "Photoelectric Mixing As a Spectroscopic Tool", Journal of the Optical Society of America, **51**(3), 253-259, 1961
10. H.Z. Cummins and H.L. Swinney, "Light Beating Spectroscopy", *Progress in optics*, E. Wolf, 135-200, North-Holland, Amsterdam, 1970
11. A. Serov, W. Steenbergen, and F. De Mul, "Prediction of the photodetector signal generated by Doppler-induced speckle fluctuations: theory and some validations", Journal of the Optical Society of America, **18**(3), 622-630, 2001
12. C.F. Bohren and D.R. Huffman, *Absorption and scattering of light by small particles*, Wiley, New York, 1998
13. A.M.K. Nilsson, P. Alsholm, A. Karlsson, and S. Andersson-Engels, "T-matrix computations of light scattering by red blood cells", Applied Optics, **37**(13), 2735-2748, 1998
14. L.O. Reynolds and N.J. Mccormick, "Approximate two-parameter phase function for light scattering", Journal of the Optical Society of America, **70**(10), 1206-1212, 1980
15. M. Hammer, D. Schweitzer, *et al.*, "Single scattering by red blood cells", Applied Optics, **37**(31), 7410-7418, 1998
16. A. Roggan, M. Friebel, *et al.*, "Optical properties of circulating human blood in the wavelength range 400-2500 nm", Journal of Biomedical Optics, **4**(1), 36-46, 1999
17. A. Kienle, M.S. Patterson, L. Ott, and R. Steiner, "Determination of the scattering coefficient and the anisotropy factor from laser Doppler spectra of liquids including blood", Applied Optics, **35**(19), 3404-3412, 1996
18. S.A. Prahl, M. Keijzer, S.L. Jacques, and A.J. Welch, "A Monte Carlo Model of Light Propagation in Tissue", SPIE Institute Series, (5), 102-111, 1989
19. W.H. Press, B.P. Flannery, S.A. Teukolsky, and W.T. Vetterling, *Numerical Recipes in C : The Art of Scientific Computing*, Cambridge University Press, 1992
20. L.G. Henyey and J.L. Greenstein, "Diffuse radiation in the galaxy", Astrophysical Journal, **93**, 70-83, 1941
21. S. Prahl, "Optical Absorption of Hemoglobin", Oregon Medical Laser Center, http://omlc.ogi.edu/spectra/hemoglobin/index.html, 1999
22. F. Habibzadeh, M. Yadollahie, M. Roshanipoor, and M. Haghshenas, "Derivation of Blood Hemoglobin Concentration from Hematocrit: A Simple Method for Rural Areas", Archives of Iranian Medicine, **4**(3), 120-122, 2001
23. V. Twersky, "Absorption and multiple scattering by biological suspensions", Journal of the Optical Society of America, **60**(8), 1084-93, 1970
24. L.H. Wang, S.L. Jacques, and L.Q. Zheng, "Mcml - Monte-Carlo Modeling of Light Transport in Multilayered Tissues", Computer Methods and Programs in Biomedicine, **47**(2), 131-146, 1995
25. H.W. Jentink, F.F.M. Demul, *et al.*, "Monte-Carlo Simulations of Laser Doppler Blood-Flow Measurements in Tissue", Applied Optics, **29**(16), 2371-2381, 1990
26. F.F. De Mul, W. Steenbergen, and J. Greve, "Doppler Monte Carlo simulations of light scattering in tissue to support laser-Doppler perfusion measurements", Technology and Health Care, **7**(2-3), 171-83, 1999
27. T.V. Starkey, "The laminar flow of streams of suspended particles", British Journal of Applied Physics, **7**(2), 52-55, 1955
28. E.C. Eckstein, D.G. Bailey, and A.H. Shapiro, "Self-diffusion of particles in shear flow of a suspension", Journal of Fluid Mechanics, **79**(1), 191-208, 1977